Biochimica et Biophysica Acta 1848 (2015) 2295–2307

Contents lists available at ScienceDirect

Biochimica et Biophysica Acta

journal homepage: www.elsevier.com/locate/bbamem

Artificial biomembrane based on DPPC — Investigation into phase transition and thermal behavior through ellipsometric techniques

Carmen M. González [a,*], Guadalupe Pizarro-Guerra [a], Felipe Droguett [a], Mauricio Sarabia [b]

[a] Departamento de Química, Universidad Tecnológica Metropolitana, Santiago 7800003, Chile
[b] Instituto de Física, Pontificia Universidad Católica de Chile, Santiago 7820436, Chile

ARTICLE INFO

Article history:
Received 22 January 2015
Received in revised form 1 July 2015
Accepted 2 July 2015
Available online 3 July 2015

Keywords:
Ripple phase
Thin films
Ellipsometric measurements
Surface wettability

ABSTRACT

Organic thin film deposition presents a multiplicity of challenges. Most notably, layer thickness control, homogeneity and subsequent characterization have been not cleared yet. Phospholipid bilayers are frequently used to model cell membranes. Bilayers can be disrupted by changes in mechanical stress, pH and temperature. The strategy presented in this article is based on thermal study of 1,2-dipalmitoyl-*sn*-glycero-3-phosphocholine (DPPC) through analysis of slight changes in material thickness.

The sample was prepared by depositing X- or Y-type DPPC bilayers using Langmuir–Blodgett technique over silicon wafer. Thus, molecular inclination degree, mobility and stability of phases and their respective phase transitions were observed and analyzed through ellipsometric techniques during heating cycles and corroborated by Grazing Incidence X-ray Diffraction and Atomic Force Microcopy measurements. DPPC functional group vibrations were detected by Raman spectra analysis. Scanning Electron Microscope with Field Emission gun (FE-SEM) and conventional SEM micrographs were also used to characterize sample morphology, demonstrating that homogenous bilayer formations coexist with some vesicles or micelles at surface level. Contact angle measurements corroborate DPPC surface wettability, which is mainly related to surface treatment methods of silicon wafer used to create either hydrophilic or hydrophobic nature regarding the substrate surface. Also, shifting and intensity changes of certain functional groups into Raman spectra confirm water presence between DPPC layers. Signal analysis detects certain interdigitation between aliphatic chains. These studies correspond to the base of future biosensors based on proteins or antimicrobial peptides stabilized into phospholipid bilayers over thin hydrogel films as moist scaffold.

1. Introduction

Cell membranes are constituted by different types of lipids–proteins that play important roles within many biological processes. Examples include, separation of cell interior from its surrounding environment, selective molecular translocation of multiple compounds and association with signal transduction, among other functions [1,2].

It follows that the most common structural unit of cell membrane are phospholipids; these compounds have both hydrophobic and hydrophilic parts (amphiphilic nature) provided by functional groups such as: sulfates, phosphates, alcohol, carboxylic acids and fatty acid tails, respectively. According to this, in aqueous environments, these types of molecules have a tendency to self-assemble into larger structures such as vesicles or liposomes, producing a bilayer membrane, entrapping internal aqueous compartment in the case of liposomes. However, these types of structures can spontaneously rupture and fuse to form supported lipid bilayers (SLBs) [3,4]; this type of arrangement is used as base for membrane models to investigate properties of biological membranes [5] and reconstituted protein machineries [6].

The most common and simple strategy to form stable SLBs is via lipid vesicle adsorption, which can occur spontaneously on a few selective surfaces (SiO_2, TiO_2 or mica). Recent studies have been focused on SLB formation produced by vesicle fusion (VF) on solid supports, using methyl-β-cyclodextrin mediated lipid exchange enriched with sphingomyelin [7], electrostatic interaction between graphene oxide (GO)/lipid membranes [8] and controlled transport of membrane protein bounds [9].

This work intended to detect interaction between 1,2-dipalmitoyl-*sn*-glycero-3-phosphocholine (DPPC) bilayer and hydrophobic/hydrophilic silicon wafer; substrate surface was modified via chemical treatments. DPPC deposition was realized through Langmuir–Blodgett technique; thin film characterization was focused on thickness measurements under heating cycles in order to detect phospholipid phase transitions.

DPPC molecules are the major component of lung surfactant in the human body. Furthermore, its composition is based on neutral lipids (primarily cholesterol, 5–10 wt.%) and proteins (5–10 wt.%). Compound largest proportion corresponds to phospholipid (~80–90 wt.%) in bilayer structure. According to this attribute, a surface

* Corresponding author.
E-mail address: carmenmabel@gmail.com (C.M. González).

http://dx.doi.org/10.1016/j.bbamem.2015.07.001
0005-2736/

pressure up to 60 mN/m produces a monolayer collapse, by fully packing upon quasi-equilibrium compression with a Langmuir–Blodgett [10], therefore this compound prevents lung alveoli from collapse at very low surface tensions. Moreover, DPPC shows different phase transitions, thus, four phases are recognized in decreasing temperature order: liquid crystalline (L_α), ripple ($P_{\beta'}$), gel ($L_{\beta'}$) and crystal subgel (L_c) phases [11], being ripple phase the most difficult to observe [12,13]. The layer integrity, in many cases, is thought to be related with water inclusion between DPPC molecules in the bilayer; however this mechanism is still not clear [14–16].

The main goal of this research is to gain information about structural arrangement and thermal characterization of DPPC bilayer (X- or Y-type deposition) over hydrophobic and hydrophilic substrates, using ellipsometry with the purpose of detect bilayer phases or phase transitions (molecular inclination and movement). X-ray Diffraction (XRD), used in grazing incidence configuration, and Atomic Force Microcopy (AFM) were used to corroborate phase transition temperatures. Raman spectroscopy was realized to DPPC multilayers (Y-type) deposited on hydrophobic and hydrophilic substrates. Scanning Electron Microscope with Field Emission gun (FE-SEM) and conventional SEM were used to visualize sample surface. Contact angle measurements were realized to corroborate the wettability.

2. Experimental

2.1. Materials

1,2-Dipalmitoyl-*sn*-glycero-3-phosphocholine semisynthetic, ≥99% (DPPC) was purchased from Sigma-Aldrich Company (St. Louise, Missouri, USA) and used without further purification. Chloroform, sulfuric acid (95–97%) for analysis Emparta®ACS. Water used in the experiments was chromatography grade LiChrosolv® which was obtained from Merck KGaA (Darmstadt, Germany). A *p* type <100> ± 0.5° orientation silicon wafer was acquired from Siegert Wafer GmbH (Aachen, Germany). Characteristics: wafer diameter 100 ± 0.3 mm, none coating, prime grade, Czochralski Crystal Growth (CZ), P/B (Boron) as dopant type, surface resistivity 10–20 Ω-cm, thickness 525 ± 20 μm, single side polished (SSP), flat/notch 2 semi-standard, total thickness variation <5 μm, bow <30 μm, warp <30 μm and particles <10 @ 0.3 μm.

2.2. Equipment and measurements

A multi-angle laser ellipsometer SE 400 Adv (SENTECH Instrument GmbH) with coupled motorized Hüber goniometers, allowing measurements between 40° and 90° in 0.5° steps, was used. Ellipsometric measurements were realized with a stabilized He–Ne laser (633 nm) which guaranteed a ±0.1 Å precision for thin film thickness measurement.

This instrument was also equipped with a home-made copper sample holder coupled with a temperature controller Model 325 (Lake Shore's Instruments) allowing heating ramps between room temperature and 70 °C. The heating system was controlled with a Pt 100 temperature sensor (PT-102-2S model, useful range 1.4 K to 873 K) and a 25 W heater (HTR-25 model), both purchased from Lake Shore's. Additionally, our ellipsometer counts with a 10× objective attached (allowing a 100× magnification added to the binoculars) that permits to align the sample with the detector and also visualizes the measure area, making possible to choose a sector with no visible big clusters or strange surface formations. Ellipsometer software, provided by SENTECH, presents Delta (Δ) and Psi (Ψ) measured values. Then, with a proper fitting, thickness value is determined for every measurement. Ψ remains almost constant for all our measurements (~34.49°). This behavior could be explained according to Drude model evolution with thickness. Thus, at low values (>10 nm), Ψ does not present important changes but Δ shows mayor variations according to theory.

Ellipsometric technique allows an accurate thickness measurement only if sample refractive index value was measured correctly, according to Santos and Arnebrant [17]. For this purpose, an Abbe Refractometer model AR4 (A.KRÜSS Optronic GmbH) was used to measure sample refractive index at different temperatures; this type of instrument allows to realize measurements in different sample states such as viscous and non-viscous liquids, powder or solid samples and mixtures. The refractometer has a yellow light source with their emission peak at λ = 589 nm, similar to He–Ne laser from ellipsometer. Refractive index measured value from an Abbe refractometer at room temperature was then interpolated according to tables for obtain refraction index at 633 nm. This technique calculates, through rotation of a prism set, the critical angle of a solution putted between two prisms; also, Amici adjustable prisms are also located in optical path with the finality to correct possible aberrations. Using this critical angle (Brewster angle) is possible to determine refraction index of studied medium.

DPPC bilayer deposition over silicon wafer substrate was realized using a single automated compression arm Langmuir–Blodgett though, Model LT-103 (MicroTestMachines), controlled by a specialized software. This equipment incorporates a tensile surface sensor and an immersion sample arm that allows the realization of an automated deposition and isotherm measurement for X-, Y- or Z-type depositions. The software possesses an integrated feedback system (closed loop) between surface pressure sensor and barrier position in order to maintain surface pressure constant during deposition process.

Certain functional groups, lattice and conformational intrachain ordering of DPPC, deposited as multilayer, were determined by Raman spectroscopy using a LabRam 010 from ISA attached to a 5.5 mW He–Ne laser (633 nm). The equipment uses a backscattering geometry, where incident beam is linearly polarized at 500:1 ratio. Objective lens used was an Olympus MPlan 50× (0.75 N.A.), which provides enough distance between objective and thin film. Measured parameters were: 750–4000 cm^{-1} (exposure time 50 s, 10 accumulations); 900–1100 cm^{-1} and 2600–3100 cm^{-1} (exposure time 75 s, 20 accumulations).

Grazing-Incidence X-ray Diffraction (GI-XRD) patterns were measured using XRD-2 beam line at the Brazilian Synchrotron Light National Laboratory (LNLS) in Campinas [18,19]. This instrument possessed a 4 + 2 circle Hüber diffractometer within its 2θ arm. The beam photon energy was fixed at 8.05 keV (1.54 Å). For XRD experiments a sample holder was also attached to a temperature variable furnace, allowing temperature variations between room temperature and 70 °C, facilitating the observation of in-situ DPPC thickness changes. Angles used in θ–2θ configuration were varied from 0.1° to 1.5° and from 0.2° to 3.0°, respectively, using 0.02° steps at 5 second exposure time per point.

To visualize and understand sample morphology and behavior under heating cycles a Digital Instruments Nanoscope III Atomic Force Microscope (AFM) at intermittent contact mode was utilized, with 125 × 125 μm maximum scan width and 5.5 μm z-hub, the resolution in z-axis was 0.03 nm [20]. AFM images were recorded using a super-sharp silicon probe (10 nm tip-radius), with 330 kHz resonance frequency and 42 Nm^{-1} spring constant. The images were treated using off-line software packages (Gwyddion) to analyze surface properties and dimensions [21]; images shown in the Results and discussion section were taken with a scan range of 10 × 10 μm. Same tip was employed in all the measurements to avoid any tip radius variation influence over surface roughness values. AFM used is located at Brazilian Nanotechnology National Laboratory (LNNano) in Campinas, Brazil.

A Scanning Electron Microscope with Field Emission gun (FE-SEM) technique was used to acquire images for DPPC thin film surface; FE-SEM had low emission current that allows measures of sample areas with much more magnification than conventional SEM, without overheating the surface and thus maintaining their biological structure. The equipment used was a JEOL JSM 6330 F microscope located at Brazilian Nanotechnology National Laboratory (LNNano) in Campinas, Brazil.

Contact angle measurements were performed in a Ramé-hart model 250 (p/n 250-U1) standard goniometer/tensiometer using sessile drop method over solid substrate. This instrument included an automated drop dispensing system. DPPC thin films (~6.0 nm) contact angle measurements were taken every 1 s.

3. Results and discussion

Two different types of silicon wafer were used in this research: *hydrophobic* and *hydrophilic*. To obtain hydrophobic type substrates, silicon wafers (as purchased from supplier) were soaked with HF solution (1%) during 2 min, followed by chromatography water wash [22]. Conversely, in order to remove the original silicon wafer native oxide, the substrates were cleaned through piranha solution (H_2SO_4:H_2O_2 in a 7:3 ratio) during 30 min at 80 °C [23]. Afterwards, they were subsequently washed with chromatography water and slightly sonicated to eliminate traces of sulfuric acid that may have remained over the silicon wafer. Finally, substrates were dried using a jet of ultra-pure nitrogen gas. Posteriorly, ellipsometric measurements were realized in order to corroborate native silicon dioxide layer thickness as an indicator for surface hydrophobicity/hydrophilicity and, also, as control for future depositions. Thus, silicon wafer treatments with HF/H_2O and H_2SO_4:H_2O_2 produce hydrophobic and hydrophilic surface, respectively. Grunder and Jacob realize measurements with electron energy loss spectroscopy (EELS) to treated silicon surfaces; their results show that hydrogen fluoride-etched (HF-etched) Si surface is covered mainly with Si–H and Si═H_2, which causes hydrophobia; Si–F in small numbers can be observed on the surface (Si–Si + HF → Si–H + Si–F) [24]. On the other hand, the procedure with piranha solution leaves 6–15 Å of hydroxylated oxide on Si surface, which prevents carbon recontamination of Si [25]. Fig. 1 shows contact angle images taken for hydrophobic (93.3°) and hydrophilic (29.6°) treated silicon wafer substrates, respectively.

3.1. Isotherm measurement — bilayer formation of DPPC using Langmuir–Blodgett as a technique

Fig. 2 corresponds to a typical curve indicating surface pressure vs free surface area per molecule for DPPC taken with Langmuir–Blodgett trough model LT-103. Surface pressure was determined through the difference between surface pressure for pure liquid medium – uncompressed with an area of 365 cm^2 (water ~72.8 mN/m) – and current pressure for compressed liquid surface, with a maximum effective compression area of 258 cm^2. This surface tension was measured by a precise pressure sensor system, which corresponded to a Wilhelmy plate (filter paper of about 14 × 14 mm), connected to a flexible reflective cantilever whose deflection is monitored by a laser — four quadrant detector system.

This type of deflection sensing system was able to detect minimal changes in cantilever position/deflection, with a resolution of no more than 0.01 mN/m. Thus, the area per molecule was calculated based on barrier position, calculated surface tension and quantity of substance dropped over the liquid surface [26,27].

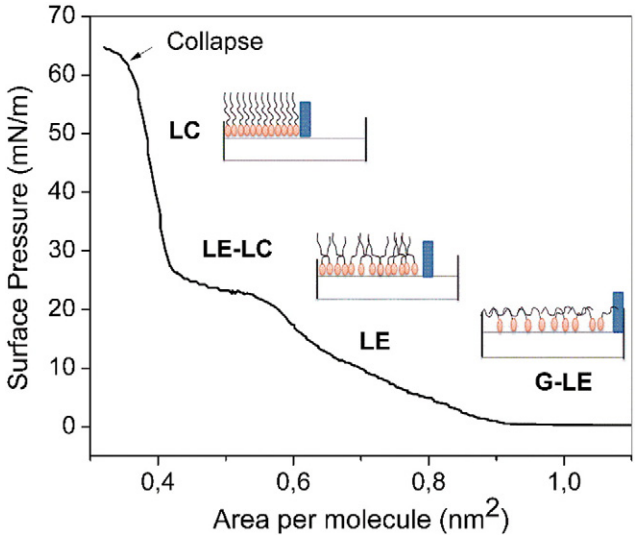

Fig. 2. Surface pressure (mN/m) vs area per molecule (nm^2) isotherm at 25 °C of DPPC on water sub-phase.

Fig. 2 shows different DPPC phases and their dependence on different factors such as surface pressure, surface area per molecule and, also, system temperature [28]. Thus, when area per lipid molecule decreased and surface pressure increases, it becomes possible to detect five different phases or phase transitions: G (gas phase), G–LE (coexistence of gas–liquid expanded phase); LE (liquid expanded phase); LE–LC (coexistence of liquid expanded–liquid condensed phase) and LC (liquid condensed phase) [29]. According to these results, the adequate pressure to form a stable monolayer over the water interface and, therefore, deposit a phospholipid layer over the substrate was 45 mN/m; above 60 mN/m monolayer collapse was expected to occur.

Langmuir–Blodgett software measures surface pressure, through Wilhelmy plate, of air–water interface during substrate immersion and emersion. Surface pressure remains constant until sample touches the air–water interface. At this point, an abrupt change in surface pressure is detected; then, surface pressure starts to continuously decrease. If substrate area is known, the amount of material transferred (transfer rate) is possible to calculate using the slope of this data. When dipper arm velocity is high (<1 mm/s), no transfer is detected; this implies that the slope of the plot surface pressure vs time during deposition is low (less than 0.5% of variation per minute is detected, commonly associated with molecular movement and solvent evaporation). When dipper arm velocity is low (>0.3 mm/s); transferring occurs at a constant rate. On these cases, the slope of surface pressure vs time is higher, more than 5% of variation per minute is detected; this means that an important quantity of material is deposited in the substrate; this procedure permits to calculate the number of deposited layers over the surface. Surface pressure sensor and compressing arm are connected forming a feedback system that allows to remain stable surface pressure during DPPC deposition (~45 ± 0.1 mN/m). Langmuir–Blodgett software

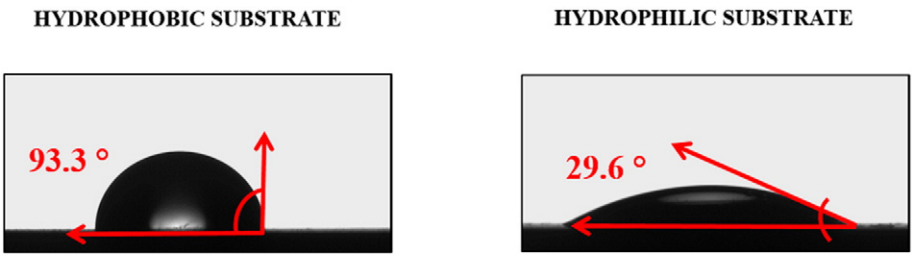

Fig. 1. Contact angle measured for hydrophobic and hydrophilic treated silicon substrates.

measures these variables and confirms a homogeneous deposition for every case.

To deposit DPPC bilayer over silicon wafer, it was necessary to dissolve 1 mg of DPPC in 0.5 mL of chloroform, then the solution was spread drop by drop with a Hamilton syringe (60 μL of solution) over pure water sub-face interface at constant room temperature (25 °C). The solution was kept at cold temperatures (−20 °C) during storage, to prevent chloroform evaporation. Before sample deposition, water/air interface with DPPC/Chloroform was allowed 20 min for solvent evaporation. After this procedure, compression was initiated at 1.51 mm/s rate and thus DPPC monolayer was transferred to silicon wafer (hydrophobic and hydrophilic types) at variable surface pressures between 45.0 and 46.5 mN/m; this value depends on isotherm obtained for each DPPC deposition, but in general the curve shape was similar to that shown in Fig. 2.

The compression speed and time allowed before compression were varied as part of the analysis. In order to deposit DPPC layers over hydrophobic or hydrophilic substrate it was necessary to vary the dipping arm speed for sample submersion and emersion.

3.2. Ellipsometric measurements

In this study, four possible phospholipid bilayer arrangements will be studied. The main difference between them was related to relative orientation of monolayers with the substrate; this conformation was mainly related to deposition speed (immersion and emersion) and also to surface properties. These different deposition arrangements will be denominated as X- or Y-type over hydrophilic or hydrophobic substrates. Before deposition procedure, DPPC solution was spread over air–water interface and isotherm was realized for every case.

Thus, to deposit X-type films over hydrophilic substrate it was necessary to quickly immerse the substrate (1.2 mm/s), DPPC was not deposited during this process; then the sample was slowly emerged (0.01 mm/s) from interface, at this moment, DPPC monolayer film was probably deposited over the surface. To deposit bilayer, this procedure was realized two consecutive times. For X-type films over hydrophobic substrate, the reverse procedure should be realized (slow immersion and quick emersion) two consecutive times to obtain the bilayer.

To deposit Y-type films over hydrophobic substrate it has to be moved slowly during the immersion (0.01 mm/s) in order to obtain a homogeneous and smooth DPPC deposition over silicon wafer. Therefore, it is necessary to emerge the sample at same immersion velocity (slow) to obtain a second DPPC monolayer deposited at backward orientation with respect to the first one. The procedure is different for Y-type film deposition over hydrophilic substrates; first a quick immersion has to be realized followed by a slow emersion; this process will probably produce a homogeneous DPPC monolayer with their polar head in contact with substrate, then a slow immersion produces a second monolayer deposition over the first one. Finally, in order to avoid a third monolayer deposition, a quick emersion has to be realized from air–water interface. Table 1 presents the different deposition type procedures; here it is possible to understand the variations between each one.

Table 1
Immersion and emersion order used in Langmuir–Blodgett deposition to reach different DPPC bilayer conformations analyzed in this study.

	Substrate polarity	1st stage (immersion)	2nd stage (emersion)	3rd stage (immersion)	4th stage (emersion)
X-type	Hydrophilic	Fast	Slow	Fast	Slow
X-type	Hydrophobic	Slow	Fast	Slow	Fast
Y-type	Hydrophilic	Fast	Slow	Slow	Fast
Y-type	Hydrophobic	Slow	Slow	N/A	N/A

Fast corresponds to dipping arm deposition velocity of 1.2 mm/s and slow to dipping arm deposition velocity of 0.01 mm/s.

DPPC sample thicknesses were precisely monitored by ellipsometric measurements. Previous studies of heating cycles using ellipsometry were realized to clean silicon wafer (hydrophobic/hydrophilic); thickness of SiO_2 layers was measured several times every 1 °C. Also, SiO_2 refraction index was changed with temperature variations according to measurements taken with the Abbe refractometer at different temperatures. In general, a low – but constant – thickness increase of SiO_2 layer was measured, leading to a thickness variation of 0.2–0.3 nm between ambient temperature and 60 °C, probably due to SiO_2 layer and silicon thermal expansion. This variation is considered at the moment of thickness calculation through Drude model.

Another important topic was the association of layer type (X or Y) with bilayer thickness; as stated previously, layer conformation was related to the polar head position or orientation, and therefore this effect determined the resultant water substrate interaction.

According to different polarity at surface level and ionic interaction of DPPC (polar/nonpolar), bilayer with different orientations should be produced [24,25]; however there is no clear evidence that the deposition variants were achieved.

While as a function of hydration level, lipid hydrocarbon chains of DPPC may be tilted in gel phase ($L_{\beta'}$) or not (L_{β}), with respect to the membrane normal plane; as water content increased, tilting angle increased as well [30]. The macroscale resultant effect of this process was thickness reduction of lipid bilayer in gel state [31].

Changes in DPPC thickness were studied by ellipsometric measurements under controlled heating cycles. As previously stated, sample refractive index was necessary to determine accurately DPPC bilayer thickness.

Using the Abbe refractometer it was possible to measure DPPC refractive index, which is found to be approximately equal to 1.48 at ambient temperature; refractive index for DPPC was also measured at different temperatures showing a slight change from 1.48 to 1.51 between 22 °C and 60 °C [32]. Ellipsometry measurements were realized between 19–26 °C (room temperature) and with a relative humidity that varies between 35–50% and ambient pressure that varies between 0.95–0.96 Atm; mean values for laboratory purposes. For each sample, three temperature ramps were realized with the intention of detect phases and phase transitions according to applied temperature. Thickness variation between phases was no more than 0.1–0.2 nm approximately; therefore a precise method for thickness measurement was required. Optical parameters (measured at room conditions), such as layer refraction index (R.I.) and thickness (Th.), that were used in Drude model are listed in Table 2. Variations with temperature were considered during ellipsometry measurements (Figs. 3–6).

In addition, ripple phase transition was most notable within initial temperature ramp measurements; this effect was associated with DPPC surface oscillations resulting in variable (unstable) thickness in ellipsometric measurements. This phase is characterized by periodic one-dimensional surface undulations at lipid bilayer top [33]. As this phase appeared prior to main melting, it must correspond to a partially lipid disorder phase. For this reason, it has been stipulated that observed undulations at lipid bilayer top level arise from periodic arrangements of linear order and disorder in lipid domains interconnected to each other by weak atomic bonds [34–36]. In addition, second and third heating ramps show a clear linear tendency during $P_{\beta'}$ phase, which correspond to an undetectable thickness change, possibly due to loss water amount and to molecular arrangements in inter-layer when it is subjected to temperature stimulus

3.2.1. Hydrophobic substrate

In Fig. 3a the sample displayed an initial thickness of 5.7 nm at 22.5 °C which then decays to 5.3 nm (differential thickness = 0.4 nm) at 55 °C, thus, temperature increase favors bilayer mobility, correspondingly sample passed through all DPPC phases from L_c to L_α.

In the first ramp it was possible to detect three plateaus between 24.5–28.0 °C, 31.5–35.6 °C and 44.6–52 °C, which could be related to

Table 2
Refraction indexes and layer thickness used in Drude model for each sample.

Sample	Silicon wafer R.I./n + *ik*[a]	SiO_2 R.I./n	SiO_2 Th./nm	DPPC R.I./n	DPPC Th./nm[b]
X-type (hydrophobic)	3.870 + *i* 0.019	1.463	2.2	1.482	~5.7
Y-type (hydrophobic)	3.870 + *i* 0.019	1.462	2.4	1.484	~6.1
X-type (hydrophilic)	3.870 + *i* 0.019	1.460	1.2	1.480	~5.0
Y-type (hydrophilic)	3.870 + *i* 0.019	1.460	1.3	1.483	~5.9

[a] Obtained from substrate manufacturer technical datasheet.
[b] These values correspond to initial measured DPPC thicknesses (Figs. 3–6).

$L_{\beta'}$, $P_{\beta'}$ and L_α phases, respectively. In addition, two phase transition temperatures were detected corresponding to $L_{\beta'}$–$P_{\beta'}$ and $P_{\beta'}$–L_α transitions, located at 28.7–31.0 °C and 36.0–44.0 °C, respectively. During these phase transitions, measures present higher associated errors due to unstable bilayer structure when transition occurs; this fact implies thickness fluctuations, due to phase coexistence. It was important to highlight that ellipsometric measurements determinate mean DPPC thickness into laser spot area (no more than 1 cm^2); this was the reason for fluctuations and increased uncertainty during phase transitions. Fig. 3b corresponds to the second and third ramps for the same sample; these plots show a slight thickness decrease at 22.5 °C, with an initial thickness of 5.5 nm, which decays to 5.3 nm at 55 °C (differential thickness = 0.2 nm). Three plateaus were detected through ellipsometric measurements and were located at 21.2–28.0 °C, 35.6–43.4 °C and 48.6–55.0 °C, corresponding to $L_{\beta'}$, $P_{\beta'}$ and L_α phases, respectively; also their respective phase transitions can be located at 28.7–35.1 °C and 44.0–48.2 °C corresponding to $L_{\beta'}$–$P_{\beta'}$ and $P_{\beta'}$–L_α transitions, respectively. Within the third ramp, it was possible to measure a thickness decrease from 5.5 nm (22.5 °C) to 5.4 nm (55.0 °C), with a thickness difference of 0.1 nm. Contrary to other ramps, it was possible to detect only two plateaus located at 20.3–29.0 °C and 37.0–50.0 °C, phases that likely correspond to $L_{\beta'}$ and L_α respectively. Furthermore, it was possible to locate their respective phase transition between these temperatures (29.4–36.4 °C).

Total DPPC differential thickness decreases as measurements were performed; in this case for the first ramp this value was equal to 0.4 nm, for the second ramp 0.2 nm and for the third ramp only 0.1 nm. These results suggested that as more heating ramps were performed to the same sample, considerable amounts of water were released to surrounding system; by implication, bilayer environment was less moist in successive or repetitive measurements. Phases and phase transition temperatures were also affected, for example, in the first and second ramps it was possible to detect a slight decrease at 20.0–22.0 °C, that was undetected during the third ramp.

This decrease was possibly and likely related to water droplets collected on the sample surface or to phase transition — and thus, as a consequence the posterior phases and phase transitions were shifted to higher temperatures with the subsequent heating process. This was clearly related to a system humectation decrease, thus water changed molecular mobility into bilayer structure. Accordingly, during the third ramp it was impossible to detect ripple phase.

DPPC bilayer deposited as Y-type displayed a large variation in bilayer thickness, phase and phase transition at different temperatures to those observed for X-type, using the same hydrophobic substrate. Accordingly, Y-type deposition probably presents a larger storage water space between layers than X-type, producing an initial bilayer thickness increase; DPPC Y-type initial thickness for the first ramp is 6.1 nm (as shown in Fig. 4a).

Fig. 4a shows a very pronounced ripple phase between 31.5 °C and 44.6 °C and total thickness variation in this range was ~0.1 nm. Afterwards, at 45.0 °C, sample thickness apparently stabilized until 49.0 °C, at this point it was possible to detect thickness decay up to 51.6 °C; this variation was probably related to L_α or fluid phase. The first plateau corresponds to $L_{\beta'}$ phase located within the range between 23.3 °C and 30.0 °C; this gel phase presented lower bilayer thickness compared with previous ripple phase. It was important to mention the increase in DPPC bilayer thickness during heating cycle; this effect was related to molecule separation/movement inherent to bilayer structure and also to molecular water movements trapped between phospholipid tails, affecting system stability, producing unstable measurements during this process. Thus, the difference between initial DPPC bilayer thickness at 22.5 °C and final thickness at 55.0 °C (6.0 nm and 5.8 nm, respectively) was 0.2 nm. Second ramp measurements did not show

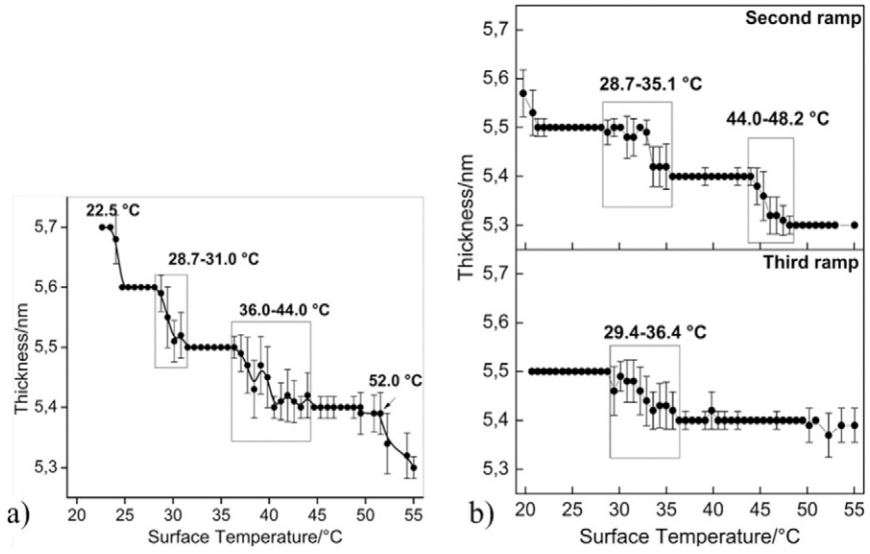

Fig. 3. Ellipsometric measurements for *X-type* depositions: a) first ramp and b) second–third ramp.

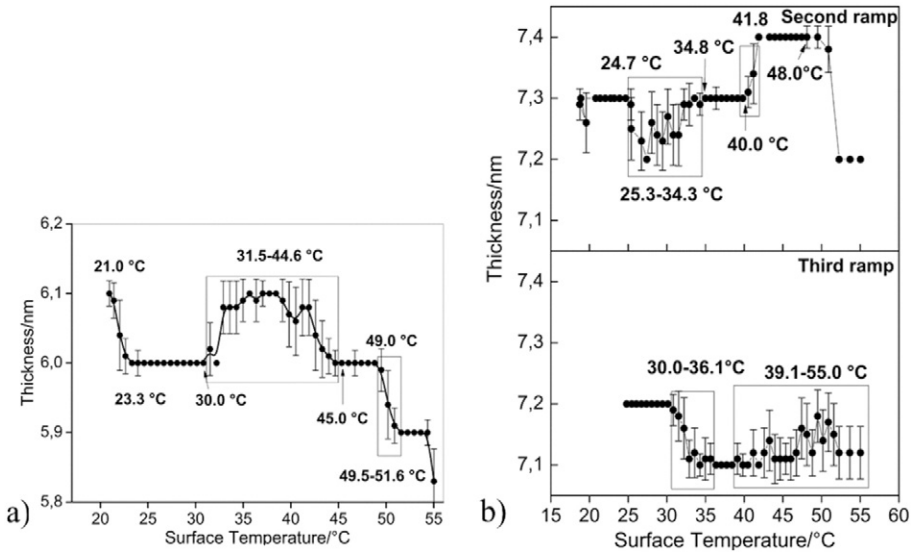

Fig. 4. Ellipsometric measurements for *Y-type* depositions: a) first ramp and b) second–third ramp.

ripple phase clearly as first ramp; however, a thickness variation between 25.3 °C and 34.3 °C was observed, that was possibly indicative of $L_{\beta'}$ phase occurrence.

At temperatures 34.8–40.0 °C and 41.8–48.0 °C there were detected two plateaus, possibly corresponding to $P_{\beta'}$ and L_{α} phases respectively; between these temperatures (40.0 °C and 41.8 °C) the respective transition was detected; a 0.1 nm thickness difference between phases was then measured through ellipsometric methods.

Finally, the third ramp resulted in a slight DPPC thickness decrease between 30.0 °C and 36.1 °C, producing a variation of 0.1 nm, from 7.2 nm to 7.1 nm. Prior to that, a short plateau was detected with further unstable phase between 39.1 °C and 55.0 °C producing thickness variation close to 0.08 nm within this range; this decrease was related only to surface sample fluency at these temperatures. It was important to emphasize that the second and third ramps did not present a detectable "ripple phases" associated a thickness variation. This behavior could be related to Y-type deposition characterized by aliphatic chains exposed to outside environment and phospholipid head group pointing at inside structure; this configuration results in the non-interaction between water and hydrophobic part of the system, preventing intra- or inter-molecular interaction at aliphatic chain level.

3.2.2. Hydrophilic substrate

X-type DPPC bilayer deposition using Langmuir–Blodgett technique presented four different plateaus located between 22.4–24.7 °C, 25.8–31.5 °C, 32.2–44.0 °C and finally between 46.1–55.0 °C. These temperatures were determined as L_c, $L_{\beta'}$, $P_{\beta'}$ and L_{α} phase limits respectively.

Total DPPC bilayer thickness variation measured between 22.5 °C and 55.0 °C was 0.3 nm; going from 4.8 nm to 4.5 nm. Each phase transition resulted in a 0.1 nm decrease in layer thickness; however it was possible to observe all differing phases and phase transitions (displayed in Fig. 5a respectively). This behavior was consistent with results founded for hydrophobic substrate, and hence was related mainly to X-type deposition.

The second ramp presents a total thickness variation of 0.3 nm (measured between 22.4 °C and 55.0 °C). These results were associated with three plateaus; temperature limits were located between 19.8–22.5 °C (corresponding to L_c phase); 23.0–28.0 °C ($L_{\beta'}$ phase)

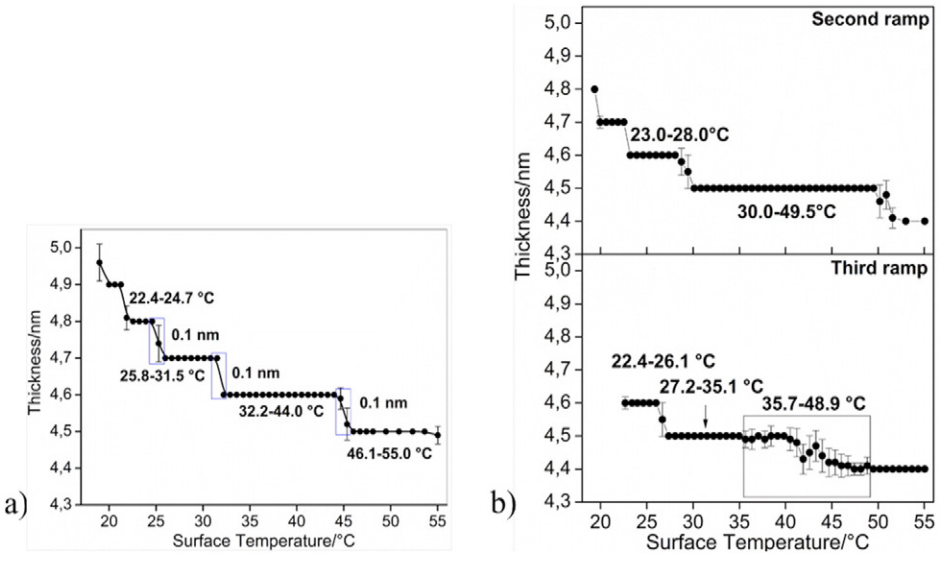

Fig. 5. Ellipsometric measurements for *X-type* depositions: a) first ramp and b) second–third ramp.

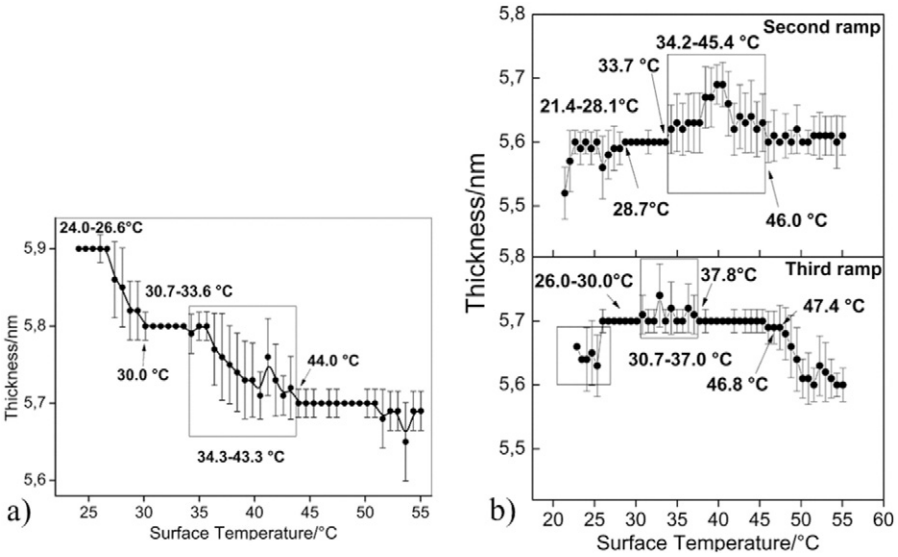

Fig. 6. Ellipsometric measurements for *Y-type* depositions: a) first ramp and b) second–third ramp.

and between 30.0–49.5 °C ($P_{\beta'}$ phase); henceforth detection of a short plateau at 51.0 °C corresponding to L_α phase. Between these values it was possible to locate their respective phase transitions, each one related to a thickness variation of no more than 0.1 nm. Finally, the third ramp showed a detectable crystalline phase L_c between 22.4–26.1 °C. After this, a slight decay of 0.1 nm was measured; furthermore, a plateau was detected from 27.2 °C to 35.1 °C, related to $L_{\beta'}$ phase. Finally, over this temperature range, higher bilayer thickness fluctuations were detected, likely related to membrane mobility and poor stability within the fluid phase (Fig. 5b).

In this type of deposition, initial thickness is generally lower in relation to Y-type (5.0 nm), independent of substrate surface property; this interesting characteristic was probably associated with water presence at layer interface, water that was mainly occluded as a consequence of sample deposition via Langmuir–Blodgett technique. In addition, aliphatic chains exposed to environmental conditions were most unstable when subjected to heating cycles, producing more interactions between them.

Fig. 6a (Y-type deposition) shows an initial plateau located between 24.0–26.6 °C, followed by a slight decay until 30.0 °C. This effect was related to $L_c \rightarrow L_{\beta'}$ transition, corresponding to a 0.1 nm thickness decrease. In addition, a second thickness decrease was located between 34.3 °C and 43.3 °C, and was attributed to ripple phase due to thickness measure high instability and, also, high associated error. During this state, thickness changes between 5.8 nm to 5.7 nm, giving a total variation of 0.1 nm. Above 44 °C, fluid phase was detectable, accompanied with a slight thickness decrease and increase in associated error.

Within the second ramp, only thickness oscillation was detectable, possibly corresponding to ripple phase initiation between 34.2 °C and 45.4 °C, variation of no more than 0.1 nm was observed; also, a high measure associated error in this sector was detected. Additionally, fluid phase (L_α) was observed above 47.4 °C and it was characterized by a slight, barely detectable, thickness decrease. Finally, the third ramp showed similar behavior compared to the second one, but with a small shift in phase and phase transition temperature, probably related to lost water amount due to previous heating cycles; the main difference between these two plots is that in the third ramp, over 47.4 °C there was a more prominent thickness decrease associated with fluid phase; also high measurement uncertainty indicates isotropic and unstable L_α phase (Fig. 6b).

In summary for ellipsometric measurements, it was found that Y-type DPPC depositions, using Langmuir–Blodgett technique, were much more well behaved – in terms of stability – than X-type due to detection feasibility of phases and phase transitions. This effect occurred during the first, second or third heating cycle, proving Y-type to be a much more stable structure than X-type bilayer. This is why this deposition type is the most widely used for phospholipid membrane formation [37–41]. Due to this, Raman Spectroscopy, GI-XRD, AFM, FE-SEM and SEM characterization methods were realized only to Y-type samples.

4. DPPC Y-type studies deposited over hydrophilic substrate

4.1. Raman spectroscopy

To characterize individually functional groups and, also, quantify disorder/order of DPPC multilayer hydrocarbon chains, Raman spectroscopy was realized. For this, it was necessary to repeat deposition process ten times in order to place DPPC multilayer (20 monolayers) through Langmuir–Blodgett over hydrophobic and hydrophilic substrates (57.3 nm and 52.9 nm, respectively). Parallel, sample was partially hydrated during deposition due to repetitive water immersion. According to previous measurements a DPPC monolayer has a thickness of ~2.7 nm; for the first case (hydrophobic) the obtained thickness is more than 20 monolayers, with a thickness excess of 3.3 nm that possibly corresponds to inter-layer water molecules. For the second case (hydrophilic) measured thickness is less than 20 monolayers, possibly due to interdigitated hydrocarbon chains. To corroborate this asseveration, 2850 cm^{-1} (methylene symmetric stretching) and 2885 cm^{-1} (methylene asymmetric stretching) intensity ratios (I_{2850}/I_{2885}, *gauche-trans* conformation) were studied. The value of peak-intensity and their ratio describe the main changes occurring in lipid hydrocarbon chain region, which is sensitive to subtle changes in conformational ordering from rotations, kinks, twists and bends of lipid chains [42].

Alternatively, a lateral order parameter (S lateral) derived from this ratio, S lateral $= [(I_{2850}/I_{2885}) - 0.7] / 1.5$ could be studied [43]. Here, $S = 1$ indicates the highest possible order and $S = 0$ indicates no order. Both parameters semi-quantitatively reflect the lateral packing of the chains.

The ratios I_{2850}/I_{2885} were 0.93 ($S = 0.15$, hydrophobic substrate) and 0.87 ($S = 0.11$, hydrophilic substrate). Thus, DPPC layers deposited on hydrophilic substrate present lower values for peak intensity ratio, associated with a decrease in *gauche* conformers, interpreted as an increase in hydrophobic interaction (chain–chain lateral) associated to a certain interdigitation. This last hypothesis is related with lower

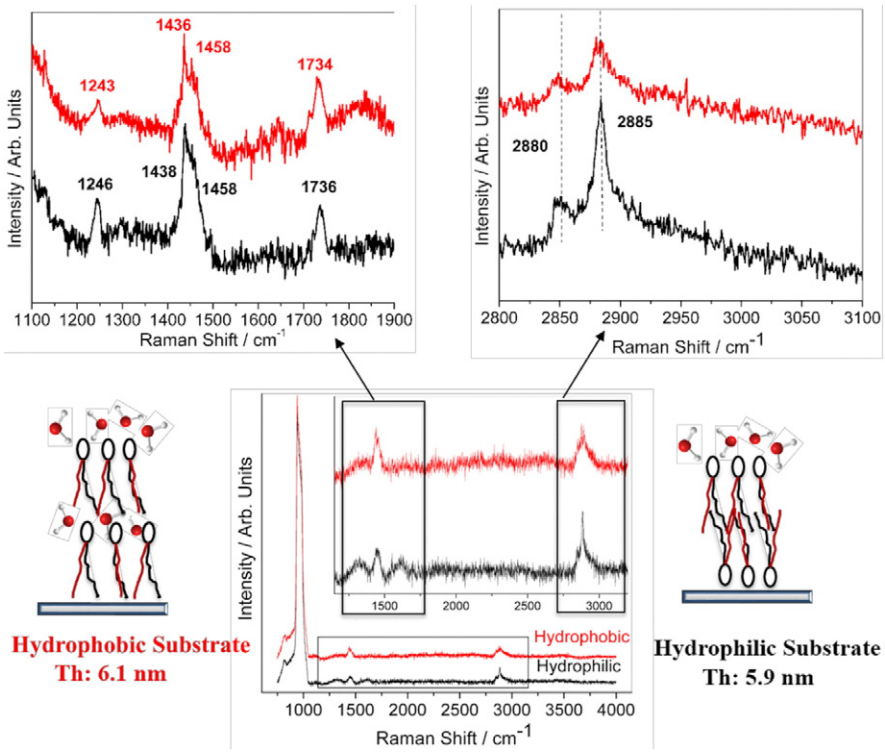

Fig. 7. a) Raman spectra of 750–4000 cm^{-1}. Higher resolution between 1100–1900 cm^{-1} and 2800–3100 cm^{-1} taken at room temperature.

thickness obtained by an ellipsometry technique (5.9 nm, Fig. 6a) in comparison to non-interdigitated DPPC deposited over hydrophobic substrate (6.1 nm, Fig. 4a) [44].

Fig. 7 shows two regions from which useful information can be derived about molecule conformation. Symmetric and antisymmetric vibration modes of $-CH_2-$ can be observed in the region comprehend between 2800–3100 cm^{-1}, which are sensitive to conformational changes as well as intermolecular interactions of lipid alkyl chains. However, $-CH_3$ stretching is not observed.

Additionally, a sharp band was observed in 1734 and 1736 cm^{-1} related to >C═O DPPC carbonyl [44]. Bush et al. conclude that changes in spectral frequencies are related with a conformational modification and lattice packing variations. Thus, it was assigned spectral features observed at 1738 and 1721 cm^{-1} in anhydrous DPPC to carbonyl stretching modes associated with lipid 1- and 2-chain positions, respectively. Thus, when molecules are hydrated, a reduction of 2-chain C═O stretching mode was shown, leaving only 1-chain C═O. This behavior is related to polar head group separation and to phosphate charge shielding with molecular water insertion [45].

The aliphatic $-CH_2-$ (high intensity) and $-CH_3$ (medium intensity) bending bands appear at 1438/1436 and 1458 cm^{-1} respectively; these bands are characteristic of inter-chain interaction; interpretation of this signal could be related to even trace amounts of water [46–48]. These bands indicate that the hydrocarbon chains are predominantly packed in a hexagonal sub-cell lattice, where each hydrocarbon chain can rotate freely around its long axis oriented perpendicularly to the film surface.

On the other hand, PO_2^- antisymmetric stretching mode for DPPC (with complete water remotion) has been previously assigned in 1253 cm^{-1}; also their shifting was discussed [45]. Our composite shown small bands at 1243 and 1246 cm^{-1}, corresponding to PO_2^- antisymmetric stretching mode hydrated (polar head groups), thus water amount present in bilayer produces frequency shift from 1253 cm^{-1} to 1243/1246 cm^{-1} (hydrophobic/hydrophilic substrate) [49]. A wide band is observed within the range of 940–980 cm^{-1} that is related to 2nd order optical photon of silicon wafer according to RRUFF data (ID: R040145); this signal is overlapped with antisymmetric N^+ $(CH_3)_3$ stretching band of choline groups. Finally, at 815 cm^{-1}, a weak band that involucres P–O–C stretching was observed.

4.2. Grazing Incidence X-ray Diffraction

The XRD studies carried out upon Y-type samples (in grazing incidence angle configuration, Fig. 8) allowed insight into parameters commonly obtained via X-ray Reflectivity (XRR) measurements [50,51]. Parameters like surface material density, critical angle and absorption coefficient were obtained; these types of characterization procedures reveal information about organization and structure that DPPC molecules acquire. DPPC (Y-type) thin films deposited over hydrophilic treated silicon wafer substrate showed critical angle near 0.3° for all the temperatures studied; to determine critical angle value it was necessary to find the angle corresponding to half maximum intensity measured for XRD spectra. With this value obtained, it was possible to determine the extinction coefficient for sample surface, $\beta = 2.05 \times 10^{-8} \pm 1.07 \times 10^{-9}$. Also refractive index via measurement of total internal reflection for high energy X-rays was founded; this value is close and just below 1.

Finally, using these results it was possible to determinate an approximate value for sample surface density, which varied between 1.855 and 2.201 g/cm^3, with a media located at 2.046 ± 0.105 g/cm^3. This density value was in concordance with the expected result for organic polymers like DPPC, that have densities between 1 g/cm^3 (water) and 3 g/cm^3 due to their chemical composition and structure based on carbonated chains.

X-ray Diffraction spectra after critical angle commonly correspond to XRR interference pattern for the analyzed sample. In our case, for some measurements at certain temperatures, it was only possible to visualize a very faint wave pattern for DPPC bilayer conformation, making layer thickness determination through this method almost impossible. This undefined interference spectrum was probably related to low sample thickness. To obtain a well-defined wave pattern a large

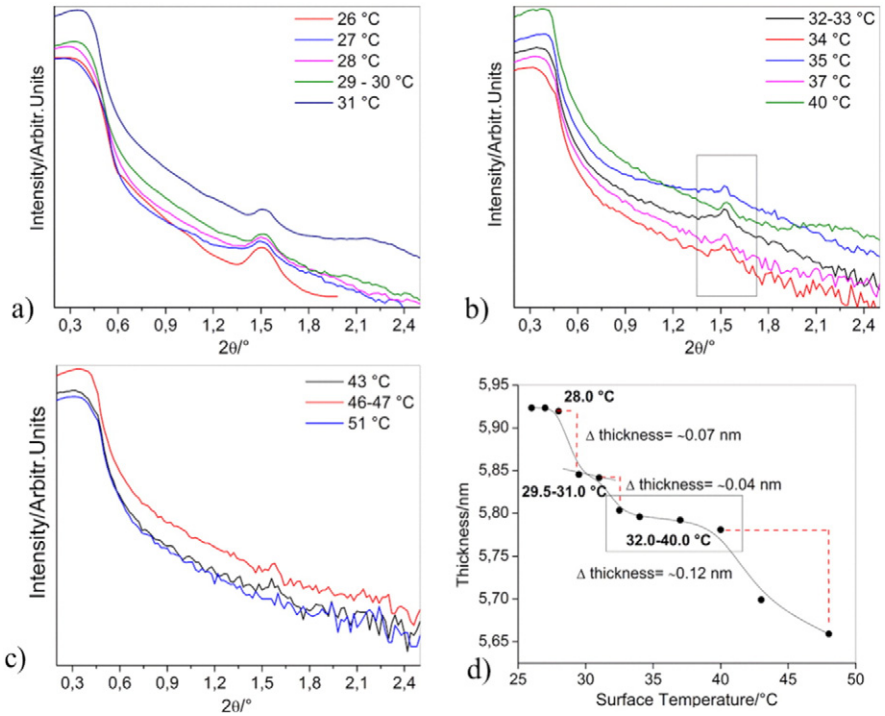

Fig. 8. a–c) XRD measurements of *Y-type* deposited DPPC bilayer over hydrophilic silicon substrate under heating cycles and d) DPPC thickness variation plot against surface temperature.

amount of crystalline ordered monolayers was necessary; two characteristics were absent from our samples.

Remarkably, for every analyzed temperature through XRD measurements it was possible to detect the first Bragg diffraction peak after critical angle, peak center value revealed important information about thin film thickness and how it varies according to system temperature.

Thus, Fig. 8a–c shows peaks located at approximately $2\theta = 1.50°$, whose position varies according to temperature; also, peak intensity and shape (Gaussian fitting) indicated system crystallinity. In this case when the temperature was raised, peak definition and intensity decreased and angle center position grew from 1.50° (26.0 °C) to 1.57° (51.0 °C); this behavior indicated a DPPC bilayer thickness modification or variation through applied temperature.

Fig. 8d presents DPPC bilayer thickness against sample surface temperature; sample thickness was calculated using Bragg's Law with n equal to 1 and λ equal to 1.54966 Å at 8 keV according to synchrotron X-ray source. Three plateaus were detected in this plot: between 26.0 °C and 28.0 °C, 29.5 °C and 31.0 °C and, finally, between 32.0 °C and 40.0 °C, which were associated with L_c, $L_{\beta'}$ and $P_{\beta'}$ phases, respectively. Thickness variation between phases corresponds to these phase transitions respectively; the difference between phase thicknesses was 0.07 nm for L_c–$L_{\beta'}$ transition, 0.04 nm for $L_{\beta'}$–$P_{\beta'}$ transition and 0.12 nm for $P_{\beta'}$–L_α transition. According to XRD spectra, between 47.0 °C and 51.0 °C, Bragg peak vanishes, indicating the loss of crystalline structure characteristic of fluid phase. These results were consistent with previous measurements obtained using ellipsometric techniques for this type of sample (Fig. 6a). However, ripple phase was undetectable using XRD measurements, probably related to long heating exposure time necessary to record this data; this condition presented difficulty in the detection of minimal changes in the molecular arrangements due to molecular accommodation with temperature. For ellipsometric measurements the elapsed time per point was no more than 3 to 5 min, for XRD measurements the elapsed time per point was approximately 40 to 50 min; this time was enough for a stable molecule accommodation in bilayer structure to be reached even in ripple phase.

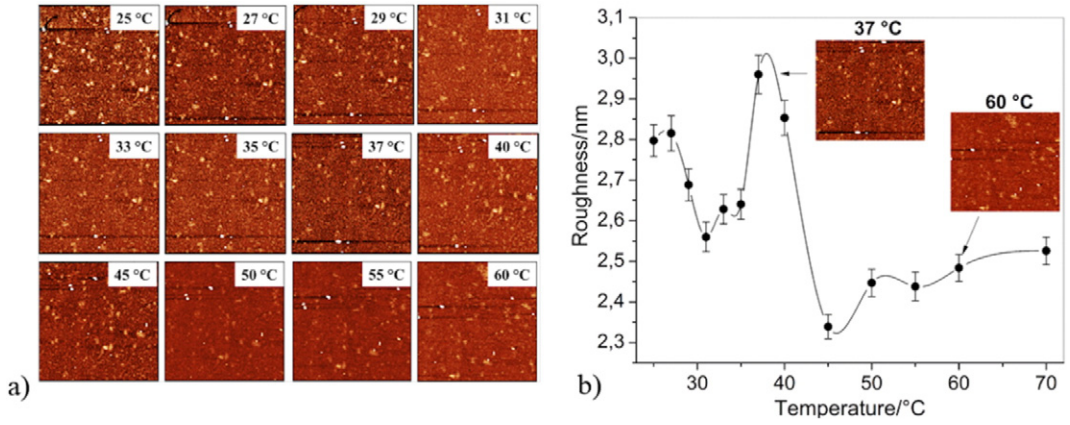

Fig. 9. Micrographs obtained with AFM technique at scan range of 10 × 10 μm under heating cycles for DPPC over silicon substrate, with their respective graph of surface roughness vs temperature.

4.3. Atomic force microscopy measurements

AFM studies proved that sample possessed distinct phases and phase transitions when bilayer was subjected to heating cycles. Fig. 9 shows a series of surface DPPC topographic micrographs ordered at increasing temperatures from 25 °C to 70 °C; these temperature intervals were chosen because the DPPC phases and phase transition temperatures were expected to be within this temperature range. Sample roughness was also obtained for each temperature. Similar studies were carried out by Gerard Oncis et al., using DPPC monolayer upon a mica substrate, revealing the presence of only one phase transition event at ~46 °C [52]. Other studies have been focused on the cholesterol concentration influence upon lipid bilayer phase transitions, using AFM-based force spectroscopy, and other characterization techniques [53–55]. These studies have drawn attention to the role of cholesterol in the regulation of cell membrane physical properties such as membrane compaction and interaction between polar heads, among others.

It is important to mention that ellipsometry measures a mean layer thickness in the area of the laser spot; this area is approximately 1 mm^2 (1×10^{-6} m^2). AFM measurements were taken in a smaller area, 100–400 μm^2 for AFM cases ($1–4 \times 10^{-10}$ m^2). Surface roughness measure by AFM is very low, meaning that in optical terms for ellipsometry techniques, sample surface is smooth.

Topographic surface images revealed homogenous and smooth films, meaning that DPPC bilayer deposition using Langmuir–Blodgett technique had produced high quality films without big cluster formations. In addition, the images acquired at 27.0 °C, 29.0 °C and 31.0 °C show a roughness decrease proving that at this temperature range, the sample remained within the same DPPC phase, although combined with certain movement in surface layer, related to the molecular inclination. Between 25.0 °C and 27.0 °C it was possible to locate a phase transition or phase coexistence between L_c and $L_{\beta'}$ phases, through the detection of visible changes in their topography, characterized by an abrupt increase in roughness.

Again these results were consistent with previous studies [12]. In the temperature range from 31.0 °C to 35.0 °C it was possible to identify a coexistence of two phases ($L_{\beta'}$ and $P_{\beta'}$); above this temperature until 45.0 °C, disintegration of small clusters was therefore detectable; this was probably related to molecule movement and reorganization at surface level due to the temperature rise; these micrographs, similar to those acquired previously, demonstrated that within this temperature range, the DPPC remained in the same phase; most likely the ripple phase. At higher temperatures, up to 45.0 °C, the topography dramatically became less rugged, implying a formation of new surface DPPC small clusters, perhaps with interdigitated or partly interdigitated lipid chains; this process was probably related to a phase transition located between 40.0 °C and 45.0 °C, but with non-surface cluster mobility. After this temperature, at 50.0 °C, 60.0 °C and 70.0 °C, surface roughness became small and remained similar in these three last micrographs, meaning that from 50.0 °C to 70.0 °C the sample remained in the same phase, and according to sample roughness, probably corresponded to fluid disorder phase (L_α).

4.4. Scanning Electron Microscopy — FE-SEM and SEM measurements

DPPC bilayer surface morphology was investigated through SEM measurements using two modalities, conventional one and with a field emission electron gun (FE-SEM). The results obtained using these techniques revealed certain surface level alignments within the samples analyzed.

The micrographs obtained through FE-SEM measurements (shown Fig. 10a–b) and SEM (in Fig. 10d) displayed a certain surface homogeneity, probably related to the technique used for the DPPC bilayer formation (Langmuir–Blodgett). However, on layer surface it was possible to observe some molecular assemblies, identified here as vesicles (a closed bilayer upon itself containing interior water) or micelles (a closed monolayer with no water in their interior). The latter structure was probable due to the humid environment existent in the system; therefore vesicles were much more likely to occur. Besides which, homogeneous bilayer formation requires added complexity, therefore the likelihood of its spontaneous occurrence was diminished.

In our case due to the deposition type, it was more likely to find bilayers than other structures; a scheme of this situation is shown in Fig. 10c. Moreover, Fig. 10d shows a micrograph taken with conventional SEM where waves or undulations at surface level were observed; this effect was attributed to the deposition method; indeed these waves were related to immersion and deposition processes and their respective rates; where bilayer deposition was realized through a controlled arm connected to an accurate step motor. Accordingly, DPPC deposition was not a continuous process as expected, and therefore it was very likely to detect these types of waves in the deposited surface.

4.5. Contact angle

To understand the wettability of DPPC thin films and silicon substrate (hydrophobic or hydrophilic) a chromatography grade water drop (highly polar) was deposited over sample surface; the DPPC bilayer over the silicon wafer and silicon wafer alone. Contact angle measurements for hydrophilic and hydrophobic silicon wafer surfaces allowed the determination of silicon hydrophilicity or hydrophobicity level; for hydrophobic silicon wafers, the initial contact angle was ~93.3°, and for hydrophilic substrates, the initial contact angle was ~29.6°, both of them measured at ambient conditions. In order to know the DPPC layer behavior when exposed to wet conditions, the contact angle was measured continuously over a period of 25 min.

Small initial contact angles (~35.6° at 0 min) correspond to high surface wettability (Fig. 11a). An automated volume dispenser is attached to a syringe during contact angle measurements. A constant volume of 10 μL was added at surface level. DROPImage software, from Rame-Hart Co., is used to acquire and analyze data obtained from the contact angle tensiometer/goniometer device. All these measurements were taken at ambient conditions (19–26 °C, relative humidity 35–50% and ambient pressure 0.95–0.96 Atm).

Fig. 11a shows five images at different times (5, 10, 15, 20 and 25 min) with their respective contact angle (red sketch) for DPPC bilayer deposited over hydrophilic substrate. Fig. 11b shows a comparison between the continued contact angle measurement of hydrophilic silicon and the DPPC over this type of substrate. These results suggest that hydrophilic silicon wafer (black line) presents a continuous decrease in their contact angle value that can be quantified according to the plot slope; for this case, contact angle decreases ~1° per minute; this value could be only related with dissolvent evaporation due to room temperature conditions (~25 °C in atmospheric pressure). Same procedure was measured for DPPC bilayer deposited over the hydrophilic substrate giving a contact angle decrease of ~0.9° per minute; this value was related mainly to the same process than the first one, spontaneous dissolvent evaporation at room conditions. According to these results, it is possible to conclude that DPPC bilayer does not absorb important quantities of water. This is concordant to expect results according that bilayer thickness is ~6.0 nm.

5. Conclusion

Ellipsometric technique proved to be an effective and accurate tool for understanding thickness changes associated with phases and phase transitions of DPPC bilayer(s). The method allowed the detection of minimal sample thickness variation with low associated error and high stability, resulting in precisely obtained data. According to these measurements, Langmuir–Blodgett technique ensured a proper and stable bilayer formation. The structural and molecular ordering was related to silicon substrate nature (hydrophobic and hydrophilic) and with the type of deposition used (X- or Y-type); however there is no

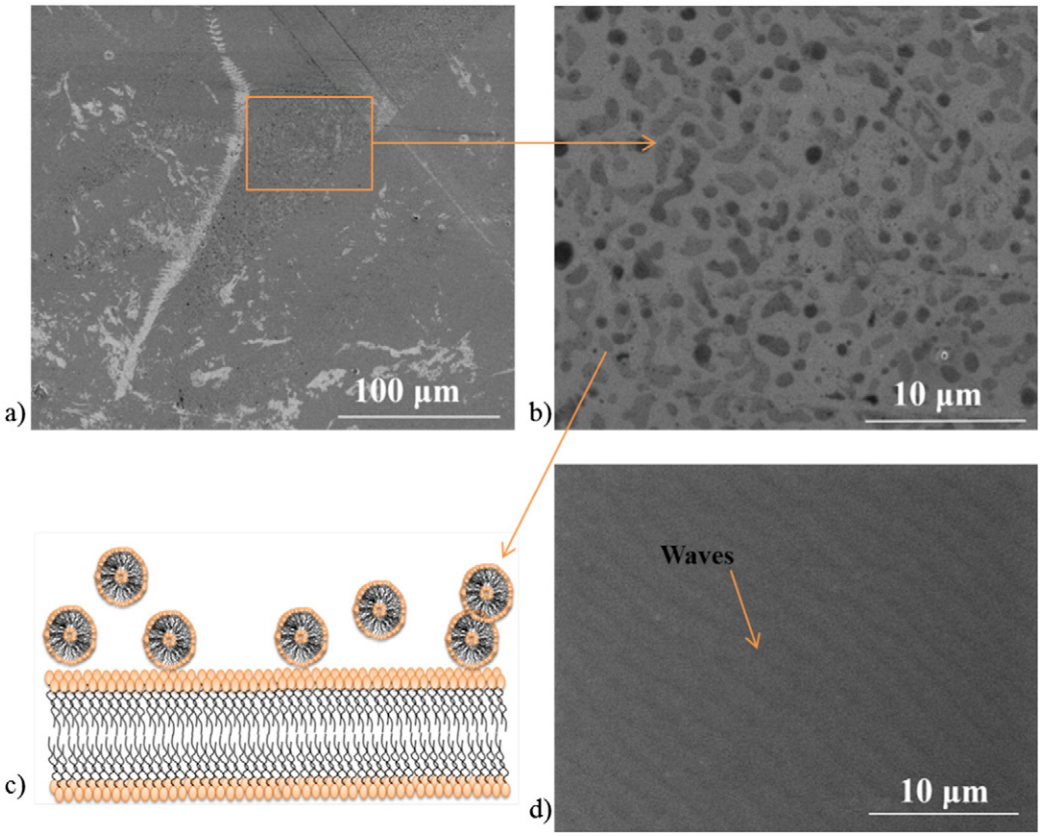

Fig. 10. Surface topography micrographies of DPPC using: a) FE-SEM (1 k× magnification); b) FE-SEM (10 k× magnification); c) scheme of bilayer-vesicle structure coexistence at surface level; and d) conventional SEM (5 k× magnification).

clear evidence if this conformations were achieved; this last characteristic was relevant for DPPC bilayer thickness due to water inclusion effects and intra- or inter-molecular interaction between monolayers that constitute the bilayer. In addition, stability and molecular movement under heating cycles were also related with orientation and ordering of aliphatic chains compared to phospholipid heads. Additionally, Raman spectral studies show some characteristic vibrations of surfactant functional groups, thus intensity ratio between methylene symmetric and antisymmetric stretching is related with hydrocarbon chains order/disorder. These values indicate certain interdigitation of aliphatic chains, when DPPC is deposited over hydrophilic substrate. Similar results were obtained by ellipsometry techniques, where a decreasing bilayer thickness was detected. Together, water insertion into bilayer was corroborated according to position of >C═O band, associated with lipid 1-chain position; also, shifting to lower wavenumber of PO^{2-} antisymmetric stretching mode and $–CH_2–$ and $–CH_3$ bending lead to the same conclusions.

The ellipsometric results obtained were analyzed in order to determine phases and phase transition temperatures for DPPC bilayer conformation. In general, for the different types of depositions and substrate nature used, a thickness variation of no more than 0.1 nm was detected for each phase. Thickness variations are also useful to compare with references. It is important to mention that after every cycle, bilayer thickness was measured in the same point in order to corroborate the stability of the membrane after a thermal cycle, corroborating that bilayer still maintains their structure. AFM studies confirmed the separate phases and their respective transition temperatures (L_c, $L_{\beta'}$, $P_{\beta'}$ and L_α) when the samples were heated. Surface homogeneity was also observed by AFM. The DPPC surfaces were studied by FE-SEM and SEM; these characterization techniques

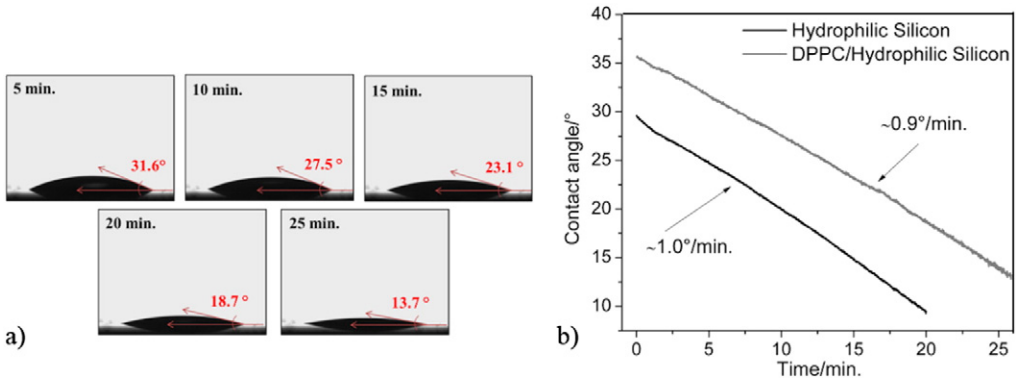

Fig. 11. a) Contact angle images for DPPC sample at different times over hydrophilic substrate and b) comparison between contact angle by hydrophilic silicon wafer (black line) and DPPC/hydrophilic silicon wafer (gray line) vs time.

revealed surface homogeneity (similar to the one obtained with AFM). Furthermore, the SEM techniques revealed a different type of surface configuration to that previously recorded, possibly constituted by a coexistence of vesicles, micelle and, mainly, bilayer structure. Besides which, some surface waves or undulations were detected that were thought to be related with the deposition methods (dipping rate used). These studies correspond to the base of future biosensors based on proteins stabilized into phospholipid bilayers over thin hydrogel films as moist scaffold.

Transparency document

The Transparency document associated with this article can be found, in the online version.

Acknowledgments

The authors acknowledge the financial support of this work by FONDECYT Grant N° 11121281 and 1110836. Dr. Gonzalez thanks to attraction and insertion of advanced human capital program, PAI 7912010031, CONICYT. Mr. Sarabia acknowledges the financial support given by CONICYT through the Magister Scholarship Grant. Authors acknowledge to LNLS-Brazilian Synchrotron National Light Laboratory for the use of grazing incidence X-ray with synchrotron source; together with LNNan—Brazilian Nanotechnology National Laboratory for the use of FE-SEM and AFM (Brazil-Campinas). Finally, authors thank Germany Academic Exchange Service (DAAD) due to ellipsometer donation.

References

[1] J.T. Groves, J. Kuriyan, Molecular mechanisms in signal transduction at the membrane, Nat. Struct. Mol. Biol. 17 (2010) 659–665.
[2] N.G. Caculitan, H. Kai, E.Y. Liu, N. Fay, Y. Yu, T. Lohmüller, G.P. O'Donoghue, J.T. Groves, Size-based chromatography of signaling clusters in a living cell membrane, Nano Lett. 14 (2014) 2293–2298.
[3] J. Andrecka, K.M. Spillane, J. Ortega-Arroyo, P. Kukura, Direct observation and control of supported lipid bilayer formation with interferometric scattering microscopy, ACS Nano 7 (2013) 10662–10670.
[4] R. Orozco-Alcaraz, T.L. Kuhl, Interaction forces between DPPC bilayers on glass, Langmuir 29 (2013) 337–343.
[5] L. Simonsson, A. Gunnarsson, P. Wallin, P. Jönsson, F. Höök, Continuous lipid bilayers derived from cell membranes for spatial molecular manipulation, J. Am. Chem. Soc. 133 (2011) 14027–14032.
[6] V. Kiessling, S. Ahmed, M.K. Domanska, M.G. Holt, R. Jahn, L.K. Tamm, Rapid fusion of synaptic vesicles with reconstituted target SNARE membranes, Biophys. J. 104 (2012) 1950–1958.
[7] I. Visco, S. Chiantia, P. Schwille, Asymmetric supported lipid bilayer formation via methyl-β-cyclodextrin mediated lipid exchange: influence of asymmetry on lipid dynamics and phase behavior, Langmuir 30 (2014) 7475–7484.
[8] H. Lei, X. Zhou, H. Wu, Y. Song, J. Hu, S. Guo, Y. Zhang, Morphology change and detachment of lipid bilayers from the mica substrate driven by graphene oxide sheets, Langmuir 30 (2014) 4678–4683.
[9] J. Neumann, M. Hennig, A. Wixforth, S. Manus, J.O. Rädler, M.F. Schneider, Transport, separation, and accumulation of proteins on supported lipid bilayers, Nano Lett. 10 (2010) 2903–2908.
[10] K.Y.C. Lee, Collapse mechanisms of Langmuir monolayers, Annu. Rev. Phys. Chem. 59 (2008) 771–791.
[11] S.L. Duncan, I.S. Dalal, R.G. Larson, Molecular dynamics simulation of phase transitions in model lung surfactant monolayers, Biochim. Biophys. Acta 1808 (2011) 2450–2465.
[12] C. González, U.G. Volkmann, M.J. Retamal, M. Cisternas, M.A. Sarabia, K.A. López, Thermal behavior of 1,2-dipalmitoyl-sn-3-phosphoglycerocholine bi- and multilayers, deposited with physical vapor deposition under ellipsometric growth control, J. Chem. Phys. 136 (2012) 134709–134714.
[13] L.M.C. Lima, M.I. Giannotti, L. Redondo-Morata, M.L.C. Vale, E.F. Marques, F. Sanz, Morphological and nanomechanical behavior of supported lipid bilayers on addition of cationic surfactants, Langmuir 29 (2013) 9352–9361.
[14] A. Sathi, V. Viswanad, T.P. Aneesh, B.A. Kumar, Pros and cons of phospholipid asymmetry in erythrocytes, J. Pharm. Bioallied Sci. 6 (2014) 81–85.
[15] S.J. Opella, Structure determination of membrane proteins in their native phospholipid bilayer environment by rotationally aligned solid-state NMR spectroscopy, Acc. Chem. Res. 46 (2013) 2145–2153.
[16] N.A. Krylov, V.M. Pentkovsky, R.G. Efremov, Nontrivial behavior of water in the vicinity and inside lipid bilayers as probed by molecular dynamics simulations, ACS Nano 7 (2013) 9428–9442.
[17] O. Santos, T. Arnebrant, Silica supported phospholipid layers doped with GM1: a comparison between different methods, J. Colloid Interface Sci. 329 (2009) 213–221.
[18] M.L. Cortez, G.A. González, M. Ceolín, O. Azzaroni, F. Battaglini, Self-assembled redox polyelectrolyte–surfactant complexes: nanostructure and electron transfer characteristics of supramolecular films with built-in electroactive chemical functions, Electrochim. Acta 118 (2014) 124–129.
[19] J. Cui, T.H. Nguyen, M. Ceolín, R. Berger, O. Azzaroni, A. Del Campo, Phototunable response in caged polymer brushes, Macromolecules 45 (2012) 3213–3220.
[20] R.F. Silva, D.R. Araújo, E.R. Da Silva, R.A. Ando, W.A. Alves, L-Diphenylalanine microtubes as a potential drug–delivery system: characterization, release kinetics, and cytotoxicity, Langmuir 29 (2013) 10205–10212.
[21] P. Klapetek, M. Valtr, D. Nečas, O. Salyk, P. Dzik, Atomic force microscopy analysis of nanoparticles in non-ideal conditions, Nanoscale Res. Lett. 6 (2011) 1–9.
[22] Q.-Y. Tong, T.-H. Lee, U. Gösele, M. Reiche, J. Ramm, E. Beck, The role of surface chemistry in bonding of standard silicon wafers, J. Electrochem. Soc. 144 (1997) 384–389.
[23] I.M. Tidswell, B.M. Ocko, P.S. Pershan, S.R. Wasserman, G.M. Whitesides, J.D. Axe, X-ray specular reflection studies of silicon coated by organic monolayers (alkylsiloxanes), Phys. Rev. B 41 (1990) 1111–1128.
[24] M. Grundner, H. Jacob, Investigations on hydrophilic and hydrophobic silicon (100) wafer surfaces by X-ray photoelectron and high-resolution electron energy loss-spectroscopy, Appl. Phys. A Mater. Sci. Process. 39 (2) (1986) 73–82.
[25] H. Huff, Into the Nano Era: Moore's Law Beyond Planar Silicon CMOS, Springer, New York, 2010.
[26] J. Yuan, C. Hao, M. Chen, P. Berini, S. Zou, Lipid reassembly in asymmetric Langmuir–Blodgett/Langmuir–Schaeffer bilayers, Langmuir 29 (2013) 221–227.
[27] E.B. Watkins, C.E. Miller, W.P. Liao, T.L. Kuhl, Equilibrium or quenched: fundamental differences between lipid monolayers, supported bilayers, and membranes, ACS Nano 8 (2014) 3181–3191.
[28] G.L. Gaines, Insoluble Monolayers at Liquid–Gas Interfaces, Interscience Publishers, New York, 1966.
[29] G. Ma, C.H. Allen, DPPC Langmuir monolayer at the air–water interface: probing the tail and head groups by vibrational sum frequency generation spectroscopy, Langmuir 22 (2006) 5341–5349.
[30] A. Tardieu, V. Luzzati, F.C. Reman, Structure and polymorphism of the hydrocarbon chains of lipids: a study of lecithin-water phases, J. Mol. Biol. 75 (1973) 711–733.
[31] M. Eeman, M. Deleu, From biological membranes to biomimetic model membranes, Biotechnol. Agron. Soc. Environ. 14 (2010) 719–736.
[32] R. Teppner, K. Haage, D. Wantke, H. Motschmann, On the internal structure of an adsorption layer of an ionic soluble surfactant. The buildup of a stern layer monitored by optical means, J. Phys. Chem. B 104 (2000) 11489–11496.
[33] M.J. Janiak, D.M. Small, G.G. Shipley, Temperature and compositional dependence of the structure of hydrated dimyristoyl lecithin, J. Biol. Chem. 254 (1979) 6068–6078.
[34] T. Heimburg, A model for the lipid pretransition: coupling of ripple formation with the chain-melting transition, Biophys. J. 78 (2000) 1154–1165.
[35] T. Heimburg, Thermal Biophysics of Membranes, Wiley, Weinheim, 2007.
[36] A.H. De Vries, S. Yefimov, A.E. Mark, S.J. Marrink, Molecular structure of the lecithin ripple phase, Proc. Natl. Acad. Sci. U. S. A. 102 (2005) 5392–5396.
[37] B. Wicklein, M. Darder, P. Aranda, E. Ruiz-Hitzky, Phospholipid–sepiolite biomimetic interfaces for the immobilization of enzymes, ACS Appl. Mater. Interfaces 3 (2011) 4339–4348.
[38] Y. Lange, S.M.A. Tabei, J. Ye, T.L. Steck, Stability and stoichiometry of bilayer phospholipid–cholesterol complexes: relationship to cellular sterol distribution and homeostasis, Biochemistry 52 (2013) 6950–6959.
[39] H.Y. Jing, D.H. Hong, B.D. Kwak, D.J. Choi, K. Shin, C.J. Yu, J.W. Kim, D.Y. Noh, Y.S. Seo, X-ray reflectivity study on the structure and phase stability of mixed phospholipid multilayers, Langmuir 25 (2009) 4198–4202.
[40] Y. Lee, I. Yang, J.E. Lee, S. Hwang, J.W. Lee, S.S. Um, T.L. Nguyen, P.J. Yoo, H.Y. Woo, J. Park, S.K. Kim, Enhanced photocurrent generation by Förster resonance energy transfer between phospholipid-assembled conjugated oligoelectrolytes and Nile red, J. Phys. Chem. C 117 (2013) 3298–3307.
[41] G. Gupta, S. Iyer, K. Leasure, N. Virdone, A.M. Dattelbaum, P.B. Atanassov, G.P. López, Stable and fluid multilayer phospholipid-silica thin films: mimicking active multilamellar biological assemblies, ACS Nano 7 (2013) 5300–5307.
[42] I.W. Levin, T.E. Thompson, Y. Barenholz, C. Huang, Two types of hydrocarbon chain interdigitation in sphingomyelin bilayers, Biochemistry 24 (1985) 6282–6286.
[43] B.P. Gaber, W.L. Peticolas, On the quantitative interpretation of biomembrane structure by Raman spectroscopy, Biochim. Biophys. Acta 465 (1977) 260–274.
[44] I.W. Levin, Raman spectroscopic study of an interdigitated lipid bilayer. Dipalmitoylphosphatidylcholine dispersed in glycerol, Biochim. Biophys. Acta 776 (1984) 185–189.
[45] S.F. Bush, R.G. Adams, I.W. Levin, Structural reorganizations in lipid bilayer systems: effect of hydration and sterol addition on Raman spectra of dipalmitoylphosphatidylcholine multilayers, Biochemistry 19 (1980) 4429–4436.
[46] T.J. OLeary, P.D. Ross, I.W. Levin, Effects of anesthetic and nonanesthetic steroids on dipalmitoylphosphatidylcholine liposomes: a calorimetric and Raman spectroscopic investigation, Biochemistry 23 (1984) 4636–4641.
[47] S. Krimm, J. Bandekar, J.T.E.a.F.M.R.C.B. Anfinsen, Vibrational spectroscopy and conformation of peptides, polypeptides, and proteins, Advances in Protein Chemistry, Academic Press 1986, pp. 181–364.
[48] L. Laporte, J. Stultz, G.J. Thomas, Solution conformations and interactions of α and β subunits of the *Oxytricha nova* telomere binding protein: investigation by Raman spectroscopy, Biochemistry 36 (1997) 8053–8059.
[49] E. Mushayakarara, N. Albon, I.W. Levin, Effect of water on the molecular structure of a phosphatidylcholine hydrate Raman spectroscopic analysis of the phosphate, carbonyl

and carbon–hydrogen stretching mode regions of 1,2-dipalmitoylphosphatidylcholine dihydrate, Biochim. Biophys. Acta 686 (1982) 153–159.
[50] J. Pignat, J. Daillant, L. Leiserowitz, F. Perrot, Grazing incidence X-ray diffraction on Langmuir films: toward atomic resolution, J. Phys. Chem. B 110 (2006) 22178–22184.
[51] M. Yasaka, X-ray thin film measurement techniques. V. X-ray reflectivity measurement, Rigaku J. 26 (2010) 1–9.
[52] G. Oncins, L. Picas, J. Hernández-Borrell, S. Garcia-Manyes, F. Sanz, Thermal response of Langmuir–Blodgett films of dipalmitoylphosphatidylcholine studied by atomic force microscopy and force spectroscopy, Biophys. J. 93 (2007) 2713–2715.
[53] L. Redondo-Morata, M.I. Giannotti, F. Sanz, Influence of cholesterol on the phase transition of lipid bilayers: a temperature-controlled force spectroscopy study, Langmuir 28 (2012) 12851–12860.
[54] S.R. Tabaei, J.A. Jackman, S.O. Kim, B. Liedberg, W. Knoll, A.N. Parikh, N.J. Cho, Formation of cholesterol-rich supported membranes using solvent-assisted lipid self-assembly, Langmuir 30 (2014) 13345–13352.
[55] S. Seghezza, A. Diaspro, C. Canale, S. Dante, Cholesterol drives Aβ(1–42) interaction with lipid rafts in model membranes, Langmuir 30 (2014) 13934–13941.